



THE UNIVERSITY *of* EDINBURGH

## Edinburgh Research Explorer

# 40Ar/39Ar age of the Rotoiti Breccia and Rotoehu Ash, Okataina Volcanic Complex, New Zealand, and identification of heterogeneously distributed excess 40Ar in supercooled crystals

### Citation for published version:

Flude, S & Storey, M 2016, '40Ar/39Ar age of the Rotoiti Breccia and Rotoehu Ash, Okataina Volcanic Complex, New Zealand, and identification of heterogeneously distributed excess 40Ar in supercooled crystals', *Quaternary Geochronology*, vol. 33, pp. 13-23. <https://doi.org/10.1016/j.quageo.2016.01.002>

### Digital Object Identifier (DOI):

[10.1016/j.quageo.2016.01.002](https://doi.org/10.1016/j.quageo.2016.01.002)

### Link:

[Link to publication record in Edinburgh Research Explorer](#)

### Document Version:

Peer reviewed version

### Published In:

Quaternary Geochronology

### Publisher Rights Statement:

This is the author's peer-reviewed manuscript as accepted for publication.

### General rights

Copyright for the publications made accessible via the Edinburgh Research Explorer is retained by the author(s) and / or other copyright owners and it is a condition of accessing these publications that users recognise and abide by the legal requirements associated with these rights.

### Take down policy

The University of Edinburgh has made every reasonable effort to ensure that Edinburgh Research Explorer content complies with UK legislation. If you believe that the public display of this file breaches copyright please contact [openaccess@ed.ac.uk](mailto:openaccess@ed.ac.uk) providing details, and we will remove access to the work immediately and investigate your claim.



# Accepted Manuscript, Quaternary Geochronology

## **$^{40}\text{Ar}/^{39}\text{Ar}$ age of the Rotoiti Breccia and Rotoehu Ash, Okataina Volcanic Complex, New Zealand, and identification of heterogeneously distributed excess $^{40}\text{Ar}$ in supercooled crystals.**

**Stephanie Flude<sup>a1</sup> and Michael Storey<sup>a2</sup>**

<sup>a</sup>Quaternary Dating Laboratory, Department of Environmental, Social and Spatial Change, Roskilde University, DK-4000 Roskilde, Denmark.

<sup>1</sup>Corresponding author. Present address: School of Geosciences, The University of Edinburgh, The Grant Institute, The Kings Buildings, Edinburgh EH9 3JW, United Kingdom. Email: [sflude@gmail.com](mailto:sflude@gmail.com); tel: +44 (0)131-650-7010; fax: +44(0)131- 650-7340

<sup>2</sup>Present address: Natural History Museum of Denmark, Øster Voldgade 5-7, 1350 Copenhagen, Denmark

**Accepted for publication December 2015**

**DOI: 10.1016/j.quageo.2016.01.002**

© 2016. This manuscript version is made available under the CC-BY-NC-ND 4.0 license <http://creativecommons.org/licenses/by-nc-nd/4.0/>

1  **$^{40}\text{Ar}/^{39}\text{Ar}$  age of the Rotoiti Breccia and Rotoehu Ash, Okataina Volcanic Complex, New Zealand, and**  
2 **identification of heterogeneously distributed excess  $^{40}\text{Ar}$  in supercooled crystals.**

3 **Stephanie Flude<sup>a1</sup> and Michael Storey<sup>a</sup>**

4 <sup>a</sup>Quaternary Dating Laboratory, Department of Environmental, Social and Spatial Change, Roskilde  
5 University, DK-4000 Roskilde, Denmark.

6 <sup>1</sup>Corresponding author. Present address: School of Geosciences, The University of Edinburgh, The Grant  
7 Institute, The Kings Buildings, Edinburgh EH9 3JW, United Kingdom. Email: [sflude@gmail.com](mailto:sflude@gmail.com); tel: +44  
8 (0)131-650-7010; fax: +44(0)131- 650-7340

9  
10 **Abstract**

11 Co-magmatic granitoid clasts erupted as part of the Rotoiti Ignimbrite (Rotoehu Tephra) contain euhedral  
12 K-feldspar and biotite crystals that protrude into miarolytic cavities and show textural evidence for growth  
13 in super-cooled conditions, thus are interpreted as growing during eruption.  $^{40}\text{Ar}/^{39}\text{Ar}$  stepped heating  
14 experiments on single K-feldspar crystals reveal the presence of heterogeneously distributed excess  $^{40}\text{Ar}$ ,  
15 preferentially released at lower temperature steps (most likely from fluid/melt inclusions), which cannot  
16 reliably be characterised by, or corrected for using isotope correlation diagrams due to mixing between  
17 three reservoirs of  $^{40}\text{Ar}$  (radiogenic, atmospheric and excess). This excess  $^{40}\text{Ar}$  component is common, but  
18 not ubiquitous, and an age population unmixing algorithm applied to single-crystal fusion data identifies a  
19 younger group of K-feldspar and biotite crystals that appear to be largely unaffected by excess  $^{40}\text{Ar}$ . This  
20 population gives a statistically robust weighted mean age of  $47.4 \pm 1.5$  ka ( $1\sigma$ ,  $n = 13$ ) and an  
21 indistinguishable inverse isochron age of  $50 \pm 3$  ka for this historically difficult to date eruption. The  
22 weighted mean age is significantly younger than previous age estimates of the Rotoiti eruption obtained by  
23 K/Ar and  $^{40}\text{Ar}/^{39}\text{Ar}$  dating of bracketing lavas, but is indistinguishable from recent  $^{14}\text{C}$  and (U-Th)/He dates  
24 and estimates based on orbital tuning and sedimentation rates constrained by  $^{14}\text{C}$  ages.

25  
26 **Keywords**

27 Rotoiti ignimbrite eruption;  $^{40}\text{Ar}/^{39}\text{Ar}$ ; excess- $^{40}\text{Ar}$ ; Taupo Volcanic Zone  
28  
29

## 30 **1. Introduction**

31 The Rotoiti ignimbrite and Rotoehu ash, erupted from the Okataina Caldera in the Taupo Volcanic Zone  
32 (TVZ) and immediately followed by the eruption of the Earthquake Flat (EQF) ignimbrite, is an important  
33 regional stratigraphic marker on the North Island of New Zealand and in the SW Pacific Ocean which has  
34 been used to correlate numerous stratigraphic sections both onshore and offshore (e.g. Berryman, 1992;  
35 Molloy et al., 2008; Nilsson et al., 2011; Shane et al., 2006). It occurs at the base of a remarkably well  
36 constrained tephra record in which all deposits have been correlated to their source vents and their  
37 distribution is well known (Shane, 2000) and so an accurate age for this deposit is particularly important for  
38 calculating both sedimentation rates and magma production and eruption rates in the TVZ and surrounding  
39 areas. Furthermore, the climatic conditions before and after the eruption are well constrained and the ash  
40 is interpreted to have been deposited during an interstadial, most likely in the middle of Marine Isotope  
41 Stage (MIS) 3 (Mcglone et al., 1984; Shane and Sandiford, 2003). However, despite 45 years of study and  
42 numerous attempts to date the eruption, the age of the Rotoehu ash still remains controversial, with  
43 recent published ages ranging from ~45 to 61 ka. In this paper we present  $^{40}\text{Ar}/^{39}\text{Ar}$  stepped heating and  
44 total fusion data for single crystals of K-feldspar and biotite from co-magmatic granitoid lithic clasts erupted  
45 as part of the Rotoiti ignimbrite and show that the eruption most likely took place at ~ 47 ka.

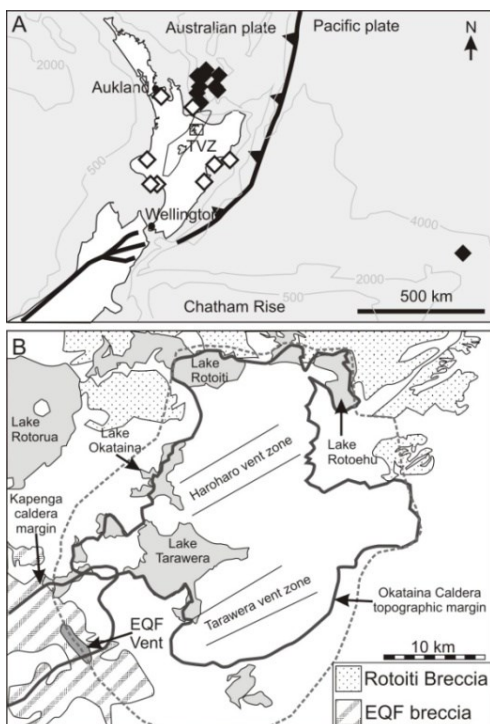
46

### 47 **1.1 Geological context**

48 The 60 km wide Taupo Volcanic Zone (TVZ) extends ~300 km north-eastwards from the centre of the North  
49 Island of New Zealand into the Bay of Plenty and the south Pacific Ocean (Figure 1). Volcanism in the TVZ  
50 began at ~2 Ma, becoming dominated by silicic volcanism after ~1.6 Ma and it is currently the most active  
51 region of silicic volcanism on Earth, with rhyolite eruption rates of  $3.8 \text{ km}^3 \text{ ka}^{-1}$  (over the last 1.6 Ma). There  
52 are at least 8 caldera complexes that have been active over the lifetime of the TVZ, with at least 34 caldera  
53 forming eruptions identified as having occurred since 1.6 Ma (Wilson et al., 1995). The Okataina caldera  
54 complex (also referred to as the Haroharo Caldera complex, Charlier et al., 2003; Shane et al., 2012; Smith  
55 et al., 2010) is one of the most productive silicic volcanoes known with rhyolite production rates quoted as  
56 being  $2.5 \text{ km}^3 \text{ ka}^{-1}$  over the last 65 ka (Wilson et al., 1995). The Rotoiti ignimbrite (also referred to as the

57 Rotoiti breccia) and Rotoehu ash were produced during the most recent caldera collapse eruption of the  
 58 Okataina caldera. The eruption began with an explosive basaltic eruption, producing the Matahina Tephra  
 59 (Pullar and Nairn, 1972) and was immediately followed by the Rotoiti eruption which produced non-welded  
 60 ignimbrite, interbedded with and overlain by phreatomagmatic ash, with the combined ignimbrite and ash  
 61 equating to a magma volume of at least 80 km<sup>3</sup> (Wilson et al, 2007). The Rotoiti eruption was followed  
 62 almost immediately (within months) by the smaller volume (7 km<sup>3</sup> of magma) Earthquake Flat ignimbrite  
 63 and associated Rifle Range ash (Nairn and Kohn, 1973; Wilson et al., 2007), which is generally considered to  
 64 originate from the Kapenga caldera complex, although Burt et al. (1998) suggested that the EQF vent  
 65 lineament represents a cryptic ring-shaped structural boundary of the Okataina volcanic centre (Figure 1B).

**Fig. 1. (A) – Map showing the tectonic setting of the Taupo Volcanic Zone (TVZ), related to the subduction of the Pacific plate beneath the Australian plate, with onshore (white diamonds) and offshore (black diamonds) occurrences of the Rotoiti Ignimbrite and / or Rotoehu ash (Allan et al., 2008; Berryman, 1992; Danišik et al., 2012; Molloy et al., 2009; Nairn and Kohn, 1973; Santos et al., 2001; Shane et al., 2006; Shane and Sandiford, 2003). Square box shows the location of Figure. 1B. (B) – Structural map of the Okataina Caldera, the source of the Rotoiti eruption (after Charlier and Wilson, 2010). Dashed line represents the cryptic structural boundary of the Okataina caldera as suggested by Burt et al. (1998).**



65 Plutonic lithic fragments brought to the surface during ignimbrite eruptions have been observed in many  
 66 TVZ volcanic deposits (Brown et al., 1998; Burt et al., 1998; Charlier et al., 2003; Ewart and Cole, 1967;  
 67 Shane et al., 2012). However, a notable class of felsic plutonic clasts contained in a lithic lag breccia facies  
 68 of the Rotoiti ignimbrite contain volcanic glass, indicating that they were incompletely crystallised at depth  
 69 and so are referred to as granitoids (Brown et al., 1998; Burt et al., 1998). The most common type of these

70 granitoid clasts, Group 1 granitoids (the subject of this study), tend to be highly friable, exhibit quench  
71 textures, such as volcanic glass, micrographic intergrowths and miarolytic cavities lined with euhedral  
72 crystals, and often contain two populations of biotite (Brown et al., 1998; Burt et al., 1998; Charlier et al.,  
73 2003). Importantly, the glass in these granitoid fragments often co-exists with euhedral crystals, implying  
74 that the glass represents quenched residual melt, rather than melt infiltration and remobilisation of a  
75 previously solidified magma body, which would result in rounded and resorbed crystals (Brown et al., 1998;  
76 Burt et al., 1998). Based on contrasting chemical and isotopic signatures, the granitoid clasts are generally  
77 considered to be co-magmatic, rather than cognate or xenolithic, to the Rotoiti ignimbrite magma, forming  
78 from a spatially close but petrogenetically distinct magma batch (possibly derived from the Matahina  
79 magmatic system) that was emplaced at a high crustal level and subsequently disturbed during the caldera-  
80 collapse phase of the Rotoiti eruption (Brown et al., 1998; Burt et al., 1998; Charlier et al., 2003; Shane et  
81 al., 2005). Cooling and crystallisation of the Group 1 granitoids is generally considered to have taken place  
82 in at least two stages, with most crystallisation taking place at 10-15 km depth, followed by volatile-loss,  
83 undercooling and crystallisation at < 3 km, associated with upheaval caused by migration of the Rotoiti  
84 magma towards the surface (Brown et al., 1998; Burt et al., 1998).

85

## 86 **1.2 Previous age estimates for the Rotoiti eruption**

87 The range of published ages for the Rotoiti eruption is given in Table 1, along with pertinent details, and in  
88 Figure 2 (all ages in this paper are quoted as  $\pm 1\sigma$ , where known). The earliest attempts to assign an age to  
89 the Rotoiti eruption utilised radiocarbon dating and were plagued by difficulties relating to the age limit for  
90  $^{14}\text{C}$  dating (generally considered to be ~40-50 ka) and contamination with younger carbon material  
91 (Froggatt and Lowe, 1990; Grant-Taylor and Rafter, 1971; Lowe and Hogg, 1995; Nairn and Kohn, 1973;  
92 Nathan, 1976; Pillans and Wright, 1992; Pullar, 1976; Pullar and Heine, 1971; Shane, 2000; Thompson,  
93 1968a; Vucetich and Pullar, 1969; Whitehead and Ditchburn, 1994). For many years, Wilson et al.'s (1992)

| Method  | Unit   | Age (ka) $\pm 1\sigma$                             | Notes   | References          |
|---|--|--|---|---------------------|
| $^{14}\text{C}$ (pre-2000)                          | Rotoiti breccia and ash  | 31 - > 41  | Ages at limit of detection and contaminated by younger carbon.  | 1-8, 10, 12, 17, 18 |
| $^{238}\text{U}$ - $^{230}\text{Th}$ disequilibrium | Rotoehu ash  | 71 $\pm$ 6   | Data considered invalid by refs 10,18   | 9                   |
| Electron spin resonance                             | Rotoiti breccia  | 45.2 $\pm$ 8.2                                     | Refs 9 and 10 suggest data may be invalid due to U-Th disequilibrium.   | 11                  |
| Marine sedimentation rates                          | Rotoehu ash  | ~55  | Tephra not conclusively identified  | 12                  |
| K/Ar  | Mayor island lava bracketing Rotoehu ash                                 | 64 $\pm$ 4   | Overlying lava = 67 $\pm$ 11 ka. Underlying lava = 63 $\pm$ 5 ka  | 13                  |
| Stratigraphic age                                   | Extrapolation between marine terrace ages formed pre and post deposition | 52 $\pm$ 7   | Ages of bracketing terraces = 40 and 59 ka. Ages of terraces refined to ~43 and 61 ka respectively by ref 21.                       | 14,15               |
| Amino acid racemization                             | Palaeosols bracketing Rotoiti breccia and ash                            | ~61  |   | 16                  |
| Optical Luminescence Dating                         | Underlying and overlying palaeosols from 2 sections                      | 42 $\pm$ 8 - 34 $\pm$ 3<br>44 $\pm$ 3 - 30 $\pm$ 2 |   | 19                  |
| $^{14}\text{C}$ -AMS                                | Wood below the Rotoehu ash   | 43.2 $\pm$ 0.6                                     |   | 20                  |
| $^{238}\text{U}$ - $^{230}\text{Th}$ disequilibrium | Rotoehu ignimbrite – xenolith:<br>Rotoehu ignimbrite - pumice            | 57 $\pm$ 8<br>> 29 $\pm$ $\frac{21}{17}$           | Whole rock – magnetite – biotite<br>Zircons   | 22                  |
| Lake sedimentation rates                            | Rotoehu ash  | 44.3   | Palynology suggests Rotoehu ash deposited during MIS 3, i.e. between 59.1 and 29.0 ka   | 23                  |
| Lake sedimentation rates                            | Rotoehu ash  | 48.9   | Composite depth scale calibrated by overlying $^{14}\text{C}$ dating of tephra  | 24                  |
| Marine sedimentation rates                          | Rotoehu ash  | ~45  | Multiple deep sea sediment cores with chronology based on $^{14}\text{C}$ and Th/U- $^{14}\text{C}$ ages of coral and foraminifera. | 25                  |
| Combined K-Ar and $^{40}\text{Ar}/^{39}\text{Ar}$   | Mayor island lava bracketing Rotoehu ash                                 | 61.0 $\pm$ 1.4                                     | Ar/Ar dates from crystals from Rotoiti and EQF eruptions give ages of 47 - 125 ka   | 26                  |
| Orbitally tuned marine sediment                     | Rotoehu ash  | 45.1   |   | 27                  |
| Lake sedimentation rates                            | Rotoehu ash  | 46-52  | Sedimentation rates extrapolated from the between overlying Maketu and Tahuna tephra layers   | 28                  |
| $^{14}\text{C}$ -AMS                                | Underlying / Overlying Rotoehu ash                                       | 47.5 $\pm$ 2.1<br>44.8 $\pm$ 0.3                   | Ages calibrated to calendar years BP  | 29                  |
| (U-Th)/He   | Rotoiti Breccia / Earthquake Flat Pumice                                 | 45.1 $\pm$ 3.3<br>45.1 $\pm$ 2.9                   |   | 29                  |

**Table 1.** Published age estimates of the Rotoiti eruption, in order of publication. 1 (Thompson, 1968b), 2 (Vucetich and Pullar, 1969), 3 (Pullar and Heine, 1971), 4 (Grant-Taylor and Rafter, 1971), 1971, 5 (Nairn and Kohn, 1973), 6 (Nathan, 1976), 7 (Pullar, 1976), 8 (Mcglone et al., 1984), 9 (Ota et al., 1989), 10 (Froggatt and Lowe, 1990), 11 (Buhay et al., 1992), 12 (Pillans and Wright, 1992), 13 (Wilson et al., 1992), 14 (Berryman, 1992), 15 (Berryman, 1993), 16 (Kimber et al., 1994), 17 (Whitehead and Ditchburn, 1994), 18 (Lowe and Hogg, 1995), 19 (Lian and Shane, 2000), 20 (Santos et al., 2001), 21 (Chappell, 2002), 22 (Charlier et al., 2003), 23 (Shane and Sandiford, 2003), 24 (Nilsson et al., 2011), 25 (Shane et al., 2006), 26 (Wilson et al., 2007), 27 (Allan et al., 2008), 28 (Molloy et al., 2008), 29 (Danišik et al., 2012)

94 age of  $64 \pm 4$  ka, based on K/Ar dating of overlying ( $67 \pm 11$  ka) and underlying ( $63 \pm 5$  ka) obsidian lava  
95 flows on Mayor Island was considered to be the most reliable age for the Rotoiti eruption. This age was  
96 subsequently revised to  $61.0 \pm 1.4$  ka based on a  $^{40}\text{Ar}/^{39}\text{Ar}$  stepped heating plateau age of  $58.5 \pm 1.1$  ka for  
97 the overlying Mayor Island obsidian lava flow and supported by stepped heating experiments on biotite and  
98 plagioclase from the Rotoiti and EQF ignimbrites, which showed a high level of xenocrystic contamination  
99 (Wilson et al., 2007). Indeed,  $^{238}\text{U}$ - $^{230}\text{Th}$  disequilibrium dating of both Rotoiti pumice and granitoid clasts  
100 and of the EQF ignimbrite indicates a prolonged crystallisation history, with isochron and weighted mean  
101 ages ranging from  $51 \pm 14.5$  ka to  $122_{-8}^{+9}$  ka (Charlier et al., 2003; Charlier and Wilson, 2010; Danišik et al.,  
102 2012). Danišik et al. (2012) addressed the problem of age-inheritance in zircons by carrying out (U-Th)/He  
103 dating, a method that has the advantage of avoiding potential pre-eruptive inheritance issues because of  
104 the high diffusion rate of  $^4\text{He}$  at magmatic temperatures. They produced indistinguishable ages of  $45.1 \pm$   
105  $3.3$  and  $45.1 \pm 2.9$  ka for the Rotoiti and EQF eruptions respectively. They also, along with Santos et al.  
106 (2001) addressed earlier problems with  $^{14}\text{C}$  dating of the Rotoiti eruption by utilising high-sensitivity  
107 Accelerator Mass Spectroscopy (AMS) and improved sample preparation procedures to remove  
108 contaminating younger carbon, producing  $^{14}\text{C}$  ages for material underlying and overlying the Rotoehu ash  
109 that are consistent with the (U-Th)/He dates. This younger date is also consistent with numerous age  
110 estimates (generally 45-50 ka) based on marine and lake sedimentation rates, calibrated by  $^{14}\text{C}$  dating of  
111 younger tephras (Allan et al., 2008; Molloy et al., 2009; Nilsson et al., 2011; Pillans and Wright, 1992; Shane  
112 et al., 2006; Shane and Sandiford, 2003) and with Optical Luminescence (OSL) dating of palaeosols above  
113 and below the Rotoiti deposits. A slightly older (but with larger errors, overlapping most other age  
114 estimates) stratigraphic age for the Rotoehu ash of  $52 \pm 7$  ka was proposed by Berryman, (1992, 1993)  
115 based on correlation of sediments bound by ages of marine terraces. The bounding terrace ages (40 ka and  
116 59 ka) were based on correlation with marine terraces at the Huon Peninsula, New Guinea, dated by  $^{14}\text{C}$   
117 and  $^{230}\text{Th}/^{234}\text{U}$  dating of corals (Chappell and Shackleton, 1986). Wilson et al. (2007) noted an updated age  
118 for the terraces (Chappell, 2002) and suggested that, according to Berryman's correlations, the Rotoiti  
119 eruption must have occurred between  $72.8 \pm 1.1$  and  $51.8 \pm 0.4$  ka. However, these ages are based on  
120 incorrect identification of the relevant marine terraces, probably due to inconsistencies in terrace naming



121 between Chappell and Shackleton (1986) and Chappell (2002); the correct age for the older terrace is 61.4  
 122 ka and the younger terrace was not re-dated, but is likely ~43 ka, based on extrapolation between older  
 123 (43.9 ka) and younger (42.1 ka) terraces, suggesting that the Rotoiti eruption took place between 61.4 and  
 124 43 ka.

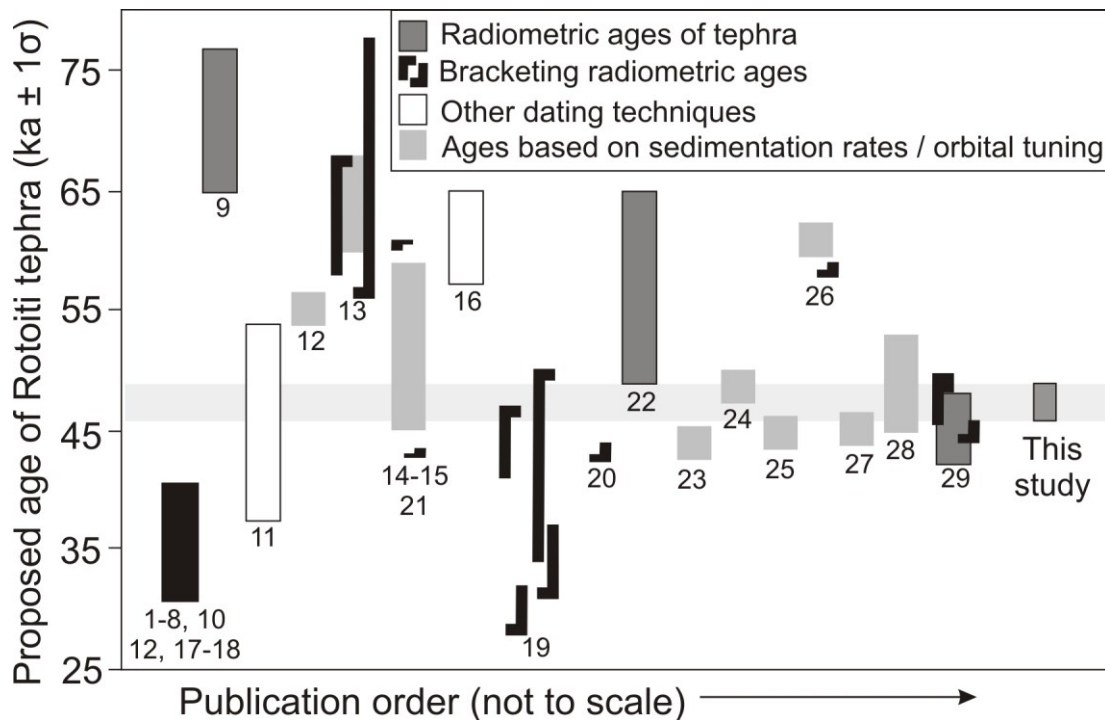


**Figure 2. Schematic diagram showing ages published for the Rotoiti eruption. Vertical bars represent 1 standard deviation of published ages, or set as arbitrary squares where errors are not available (12, 16, 23-25, 27). Numbers refer to the references cited in Table 1. The horizontal grey bar represents the age  $\pm 1 \sigma$  determined in this study.**

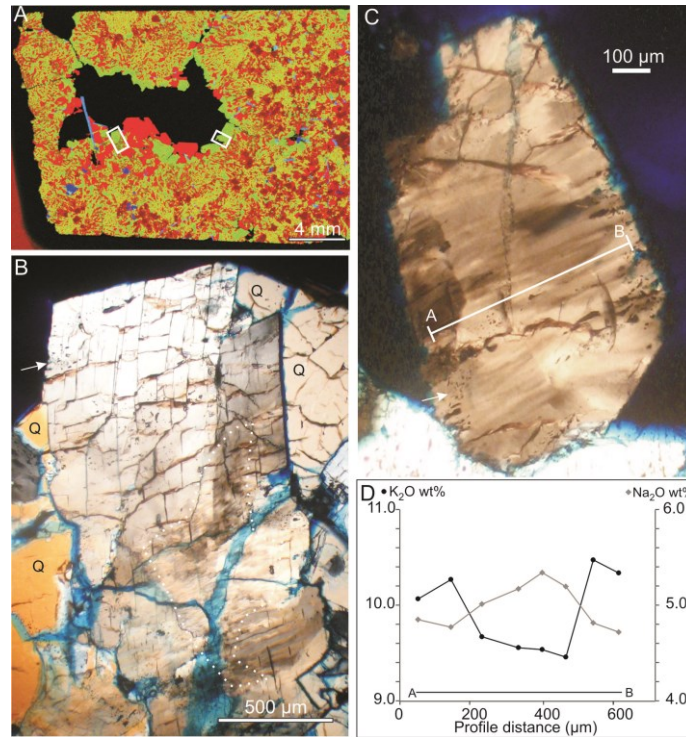
124 **2. Samples and methodology**

125 Despite evidence of pre-eruption age zircons and thus an extended crystallisation history of Group 1  
 126 granitoid fragments (Charlier et al., 2003), the abundant quench textures which they exhibit indicate that at  
 127 least part of the clasts crystallised during eruption. Sample 103/1, collected from the same granitoid block  
 128 as sample 103/2, analysed by Charlier et al. (2003), contains abundant glass and miarolytic cavities lined  
 129 with euhedral K-feldspar, quartz and biotite, which we interpret as having crystallised and quenched during  
 130 eruption.

131 A polished thin section was prepared by impregnating a split of the sample with blue epoxy to highlight the  
132 miarolytic cavities and porosity of the sample. This section (Figure 3) exhibits many of the quench features  
133 identified by Burt et al. (1998) and Charlier et al. (2003), such as granophyric texture, along with euhedral  
134 quartz and K-feldspar crystals forming linings to the miarolytic cavities. Optical petrography of the euhedral  
135 K-feldspars shows that they are highly strained, exhibiting strongly developed cleavage planes, patchy,  
136 streaky and undulose extinction and, in some crystals, kinked cleavage planes and fine-scale structures in  
137 the core of the crystal, that appear streaky under both PPL and XPL (Figure 3B). These structures are similar  
138 in appearance to plagioclase-alkali feldspar intergrowths, and patchy extinction and sector zoning formed  
139 during sanidine crystallisation from an undercooled melt (Lofgren and Gooley, 1977). We interpret these  
140 feldspar textures as representing a combination of crystallisation during melt undercooling, and  
141 deformation during shearing processes during mobilisation and eruption, a process considered to be  
142 ubiquitous in the Group 1 granitoids (Brown et al., 1998; Burt et al., 1998).

143 Element mapping and semi-quantitative spot analyses were carried out on the polished section using a  
144 Bruker-nano M4 Tornado benchtop micro-XRF system. Analysis conditions, a summary of the technique and  
145 all semi-quantitative data are given in the supplementary information and Supplementary Data Table S1. A  
146 major element map displaying Si, K and Fe is shown in Figure 3A. The large area (1.5 ×2.5 cm) covered by  
147 the x-ray map reveals that many of the granophyric intergrowths radiate towards the miarolytic cavities,  
148 often terminating with euhedral quartz and K-feldspar crystals that project into the cavity.

149 A semi-quantitative chemical composition profile across a euhedral K-feldspar crystal (Figure 3D) suggests  
150 cryptic normal zoning, with relative Na-enrichment in the core and K-enrichment at the rim. Spot analyses  
151 of the fine-scale structures in Figure 3b indicate a relative enrichment of CaO and Na<sub>2</sub>O and depletion of  
152 K<sub>2</sub>O, consistent with our interpretation that they represent plagioclase – K-feldspar intergrowths during  
153 undercooling.



155

156 **Figure 3. A)  $\mu$ -XRF element map from a polished section of a miarolytic cavity in a granitoid clast.**  
 157 **Elements are displayed as Si = red, K = green and Fe = blue, therefore quartz displays as bright red, K-**  
 158 **feldspar as green, plagioclase as dark red and biotite and Fe-oxides as blue. White boxes show the**  
 159 **positions of panels B (left) and C (right). B) XPL photomicrograph of an alkali feldspar crystal protruding**  
 160 **into the miarolytic cavity. The white dotted line highlights fine-scale textures interpreted as plagioclase –**  
 161 **K-feldspar intergrowths. Q = quartz crystals. C) XPL photomicrograph of an alkali feldspar crystal that**  
 162 **grew into the miarolytic cavity. The crystal displays streaky and patchy extinction. The line a-b shows the**  
 163 **position of the semi-quantitative chemical profile shown in panel (D) (see supplementary information for**  
 164 **details). In the photomicrographs, white arrows highlight regions in the crystals rich in fluid and / or**  
 165 **magmatic inclusions. Blue colouration is from impregnation during section preparation and highlights the**  
 166 **permeable nature of the granitoids.**

167

168 0.5-1 mm euhedral K-feldspar and 1-2 mm biotite crystals were hand-picked from miarolytic cavity linings  
 169 of the kind illustrated in Figure 3A and prepared for irradiation for Ar-isotope analysis using standard  
 170 techniques (see supplementary information). Given the likely extended crystallisation history of the  
 171 granitoid clasts, all Ar-isotope analyses were carried out on single crystals to enable identification of any  
 172 crystals that record pre-eruptive ages and prevent mixing of crystal populations. We carried out a

173 combination of single grain fusion and single grain stepped heating experiments on both K-feldspar and  
174 biotite crystals using a 50 W Synrad CO<sub>2</sub> laser. Gas clean-up was through an all-metal extraction line with a -  
175 130 °C cold trap, to remove H<sub>2</sub>O, and two water-cooled SEAES GP-50 getters to absorb reactive gases. The  
176 Ar-isotope analyses were carried out on a Nu Instruments Noblesse multi-collector noble gas mass  
177 spectrometer. Analytical procedures, previously documented in Brumm et al., (2010) are detailed in the  
178 supplementary information file and all results, correction factors and constants are given in the  
179 supplementary data file. As previous studies on similar material (Wilson et al., 2007) had reported high  
180 levels of contamination with Cl, which can cause an isobaric interference with <sup>36</sup>Ar in the mass  
181 spectrometer by formation of <sup>1</sup>H<sup>35</sup>Cl, <sup>35</sup>Cl was measured in addition to the Ar-isotope analyses to monitor  
182 for Cl contamination, none of which was observed.

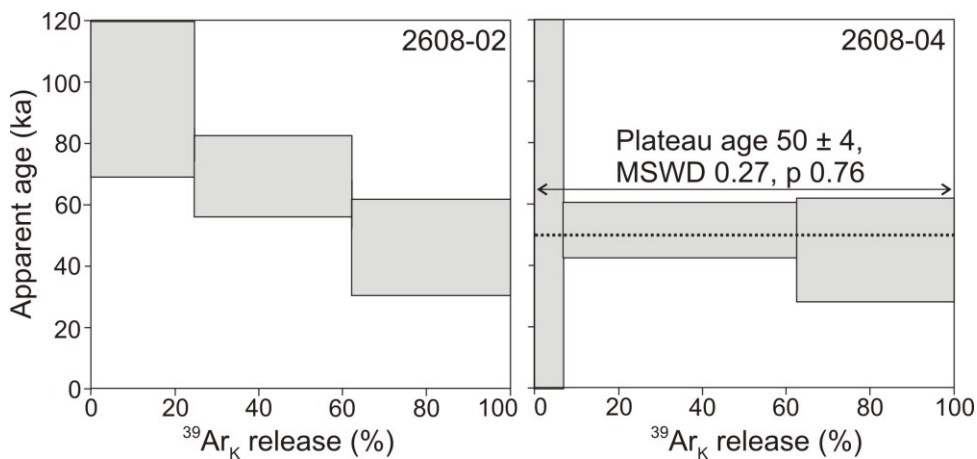
### 183 **3. <sup>40</sup>Ar/<sup>39</sup>Ar Results**

184 Results of the Ar-isotope single crystal analyses are given in supplementary Tables 2 and Figures 4 - 7. K-  
185 feldspar single grain fusion ages (excluding data with blank-corrected <sup>40</sup>Ar yields of less than 0.5 mV  
186 (~30,000 cps) and zero <sup>40</sup>Ar\* yields; n = 27) range from 31 ± 5 ka to 125 ± 18 ka, indicating that some grains  
187 record pre-eruption model ages, i.e. they are either xenocrystic or contain excess <sup>40</sup>Ar. Biotite single grain  
188 fusion ages (n=4) range from 39 ± 8 ka to 57 ± 6 ka. An isotope correlation diagram plotting all of the single  
189 crystal fusion data (Figure 5) gives an inverse isochron age of 55.3 ± 1.8 ka.

190 Stepped heating experiments were carried out on 5 K-feldspar and 1 biotite crystals, yielding 3 steps for the  
191 K-feldspars and 4 steps for the biotite, although some of these steps produced exceptionally low <sup>40</sup>Ar, <sup>40</sup>Ar\*  
192 and / or <sup>39</sup>Ar gas yields. The individual step heating data yielded apparent ages from 39 ± 8 ka to 105 ± 16  
193 ka.

194 Three of the five K-feldspar crystals gave high apparent ages for the first temperature step (up to 105 ka)  
195 and exhibit decreasing age with increasing temperature (e.g. 2608-02, Figure 4) while a fourth followed the  
196 same pattern but the first and final temperature steps yielded < 0.5 mV <sup>40</sup>Ar and so have been discounted.  
197 Isochrons could not be calculated for these crystals. Stepped heating of K-feldspar 2608-04 yielded

198 consistent ages for all three temperature steps, giving a 3-step "plateau" age of  $50 \pm 4$  ka (Figure 4) and a 3-  
 199 point isochron age of  $51 \pm 0.5$  ka ( $^{40}\text{Ar}/^{36}\text{Ar} = 298 \pm 3$ , MSWD = 0.5,  $p = 0.48$ ). Stepped heating was  
 200 attempted on one biotite crystal using 4 temperature (laser power) steps. The first two of these steps  
 201 released gas with an  $^{40}\text{Ar}/^{36}\text{Ar}$  composition within uncertainty of the atmospheric ratio of 298.56, and can  
 202 be attributed to the release of loosely adhering atmospheric argon from gentle heating of the crystal.



203

204 **Figure 4.  $^{40}\text{Ar}/^{39}\text{Ar}$  age spectra from stepped heating experiments on single K-feldspar crystals. Crystal**  
 205 **2608-02 shows a gas release pattern of decreasing model age with increasing temperature and suggests**  
 206 **that excess  $^{40}\text{Ar}$  is present in fluid and magmatic inclusions in the crystals. By contrast, crystal 2608-04**  
 207 **exhibits a flat release spectrum and younger age, suggesting that it is either unaffected by, or at least less**  
 208 **influenced by excess  $^{40}\text{Ar}$ . Error boxes on the spectra are  $2\sigma$  and all quoted errors are  $1\sigma$ .**

209

210  $^{40}\text{Ar}/^{39}\text{Ar}$  ages from stepped heating of individual crystals that vary beyond normal analytical uncertainties  
 211 can be interpreted in terms of excess  $^{40}\text{Ar}$ , inherited  $^{40}\text{Ar}$  in xenocrystic or antecrystic cores, or as  $^{39}\text{Ar}$  loss  
 212 due to recoil. These possibilities are discussed below.

#### 213 4. Interpretation of variable model $^{40}\text{Ar}/^{39}\text{Ar}$ ages

##### 214 4.1 Inherited $^{40}\text{Ar}^*$ .

215 Inherited  $^{40}\text{Ar}^*$  is a possible reason for older ages observed in both stepped heating and fusion analyses.

216 The granitoid clasts are interpreted as having crystallised in multiple stages (Brown et al., 1998; Burt et al.,

217 1998) and contain zircons that record pre-eruption ages (Charlier et al., 2003) and so it would be expected  
218 that these clasts contain antecrystic material. However, we purposefully selected crystals lining miarolytic  
219 cavities in the clasts to avoid antecrysts retaining  $^{40}\text{Ar}^*$  older than the eruption. The bulk of sample 103/1  
220 has a sugary, friable texture, indicative of gas exsolution and quenching of interstitial melt to form volcanic  
221 glass. The glass was considered by Brown et al., (1998) to be interstitial melt, rather than infiltrated melt or  
222 partial melt during reheating based on textural and chemical analysis. The presence of glass quenched from  
223 interstitial melt indicates that the granitoid remained partially molten until eruption and will have sustained  
224 elevated temperatures; Brown et al., (1998) suggested a feldspar thermometry crystallisation temperature  
225 of 700 °C for the later stage, supercooled crystals. Granophyric texture (Figure 3) and miarolytic cavities  
226 are further evidence that this sample crystallised and quenched during transport to the surface (Brown et  
227 al., 1998; Burt et al., 1998) and it is difficult to envisage a scenario where miarolytic cavities and glass could  
228 form in the subsurface and be retained over geochronologically significant timescales without being  
229 modified.

230 If the crystals we analysed did form thousands of years before the eruption and retained a portion of their  
231  $^{40}\text{Ar}^*$ , we would expect this to be reflected in the age spectra produced by stepped heating experiments.  
232 Inherited  $^{40}\text{Ar}^*$  would diffuse out of the crystal while ever the crystal is held at elevated temperature in the  
233 subsurface and / or during eruption and so the highest concentration of  $^{40}\text{Ar}^*$  would be in the core of the  
234 crystal. This would manifest on age spectra as younger ages in the early steps and older ages in the latter  
235 steps. This pattern is opposite to what is observed for stepped heating of single feldspar crystals, which  
236 produce the oldest ages in the earliest steps.

237 As a further check, we carried out diffusion modelling to assess whether a feldspar that crystallised as part  
238 of a partially molten mush, thousands of years before the eruption, would retain any  $^{40}\text{Ar}^*$  and thus give  
239 older ages. We considered a simplified scenario where an Ar-bearing feldspar was held at 700 °C and  
240 modelled the fractional Ar loss experienced by the crystal. We assumed a spherical crystal of radius of 0.5  
241 mm (the largest crystals analysed),  $D_0 = 0.0098 \text{ cm}^2 \text{ s}^{-1}$  and  $E = 44 \text{ kcal mol}^{-1}$  (Foland, 1994) and used the  
242 fractional loss equations given in McDougall and Harrison (1999). Under these conditions, 100% of the Ar in

243 the crystal would have been lost after just 40 years. Feldspars of this size that crystallised thousands of  
244 years before the eruption would only retain a significant proportion (>50%) of their  $^{40}\text{Ar}^*$  at temperatures <  
245 500 °C; the evidence for interstitial melt in the granitoid clasts is not consistent with such low  
246 temperatures.

247

#### 248 **4.2 Recoil of $^{39}\text{Ar}$**

249 Recoil of  $^{39}\text{Ar}$  during neutron irradiation may result in ejection of  $^{39}\text{Ar}$  atoms from the crystal lattice and can  
250 be a problem for samples where the grain size is approaching the  $^{39}\text{Ar}$  recoil distance (partial depletion  
251 layer thickness of 0.7  $\mu\text{m}$  - (Jourdan et al., 2007)). Recoil typically manifests on age spectra as a stepwise  
252 decrease in age with increasing temperature, similar to that observed during stepped heating of our  
253 individual feldspar crystals; gas release from early temperature steps is dominated by that from the smaller  
254 grain sizes most affected by recoil and the relative depletion in  $^{39}\text{Ar}$  relative to  $^{40}\text{Ar}^*$  results of over-  
255 estimation of the  $^{40}\text{Ar}/^{39}\text{Ar}$  age.

256 In the case of our Rotoiti samples, individual crystals are  $\sim 1\text{mm}$  diameter or larger; many appear fractured  
257 in thin section (Fig. 3B) but these fracture domains are still tens of microns in diameter and thus unlikely to  
258 be affected by recoil. It is possible that the observed patches of streaky extinction and very fine lamellae in  
259 some of the K-feldspar crystals represent structures that could facilitate recoil of  $^{39}\text{Ar}$ , but these often occur  
260 as discrete patches interspersed with areas that are more homogenous and it is likely that such a scenario  
261 would not produce the “classic” decreasing age spectrum associated with recoil.

#### 262 **4.3 Excess $^{40}\text{Ar}$**

263 Excess  $^{40}\text{Ar}$  hosted in melt or fluid inclusions may produce age spectra with older apparent ages in the early  
264 temperature steps; decrepitation of the inclusions releases the excess  $^{40}\text{Ar}$  during the earliest heating  
265 stages and contributes to the classic “saddle-shaped” age spectrum associated with excess  $^{40}\text{Ar}$ .

266 The age spectra produced by stepped heating of individual crystals (Fig. 4) are consistent with fluid /  
267 magmatic inclusion-hosted excess  $^{40}\text{Ar}$ . Furthermore, many K-feldspars in sample 103/1, contain an  
268 abundance of magmatic and / or fluid inclusions (Figure 3).

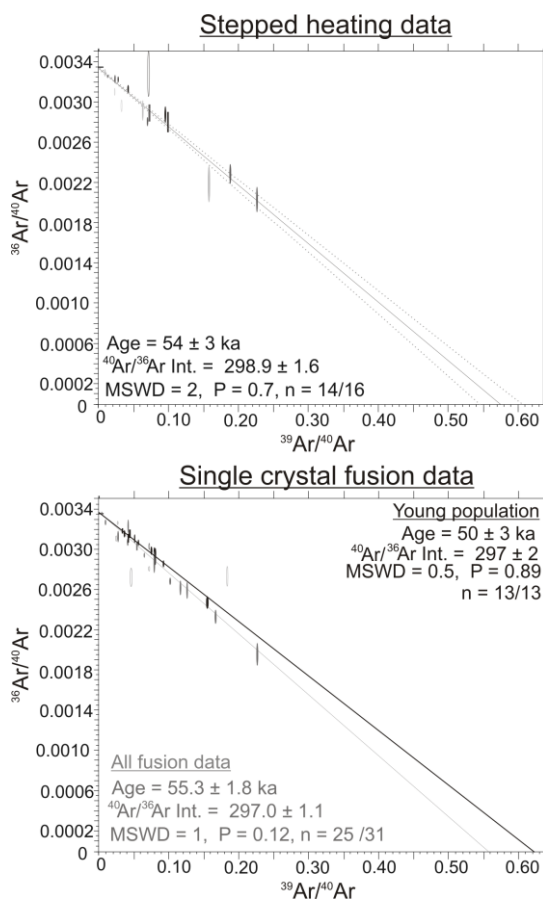
269 The stepped heating data suggest that this excess  $^{40}\text{Ar}$  is present in varying degrees in many, but not all of  
270 the crystals; the flat release and younger apparent age of crystal 2608-04 suggests that it contains little or  
271 no excess  $^{40}\text{Ar}$ . If excess  $^{40}\text{Ar}$  is inhomogeneously distributed within a sample (e.g. in clusters of fluid or  
272 magmatic inclusions, as observed in the photomicrographs in Figure 3), especially if it is decoupled from an  
273 atmospheric component (i.e. 3-way mixing between radiogenic, atmospheric and excess Ar), it can be  
274 difficult or impossible to identify using isotope correlation diagrams as regressions of the data will tend to  
275 yield an atmospheric intercept and an apparent age that is too old (Kuiper, 2002).

#### 276 **4.4 Eruption age vs. excess $^{40}\text{Ar}$ age**

277 Plotting the stepped heating data from all six (5 K-feldspar, 1 biotite) crystals onto an isotope correlation  
278 diagram produces an apparent age of  $54 \pm 3$  ka with a trapped  $^{40}\text{Ar}/^{36}\text{Ar}$  content of  $298.9 \pm 1.6$  ( $n=14/16$ ,  
279 two data points automatically rejected by the Mass Spec software). In Figure 5 the data are plotted  
280 according to their temperature step; low temperature steps (light grey) tend to lie below the isochron line  
281 while the higher temperature steps (black) lie on or above the line. The isochron has an atmospheric  
282 intercept, despite an excess  $^{40}\text{Ar}$  component clearly being identified on age spectra. Such a distribution of  
283 data points is consistent with a scenario involving mixing of atmospheric, radiogenic and excess  $^{40}\text{Ar}$ , as  
284 described by (Kuiper, 2002). Data points not affected by excess  $^{40}\text{Ar}$  would define an isochron formed by a  
285 mixing line between radiogenic and atmospheric end-members, with an atmospheric intercept.  
286 Heterogeneous incorporation of excess  $^{40}\text{Ar}$ , as a source of trapped Ar additional to atmosphere, shifts the  
287 data points downwards and to the left of the isochron line. This has the net effect of increasing the slope of  
288 the calculated isochron line, resulting in an older age, whilst maintaining an atmospheric intercept; such an  
289 apparent isochron is an artefact and does not represent mixing between a single trapped and radiogenic  
290 end members (Kuiper, 2002). The high MSWD (2) suggests that the scatter of the data is greater than would  
291 be expected based on the errors on the individual data points and this is consistent with this interpretation



292 of variably-distributed excess  $^{40}\text{Ar}$ . Inspection of the stepped heating isochron shows that it is dominated by  
 293 data from the middle and high temperature steps. Given that the middle temperature steps may still  
 294 contain excess  $^{40}\text{Ar}$ , this isochron age is considered to be an over-estimate and an upper limit of the  
 295 eruption age.



296

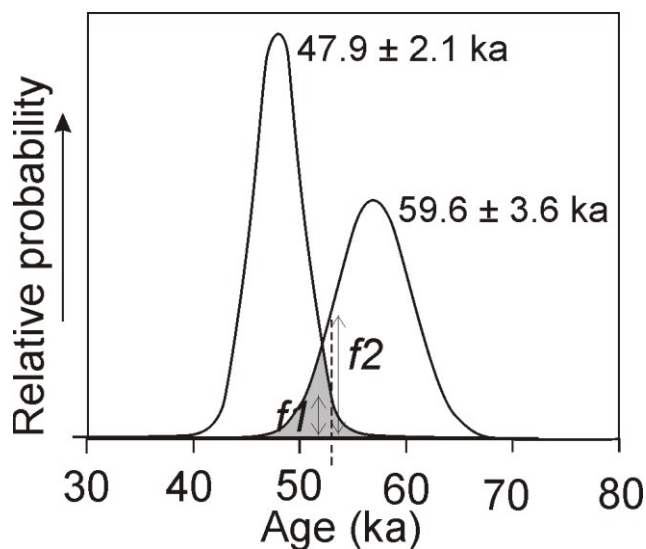
297 **Figure 5: Isotope correlation diagrams created using the software Mass Spec (Al Deino, Berkeley**  
 298 **Geochronology Center). Isochron ages were calculated invoking an automated data filtering process to**  
 299 **eliminate outliers on the basis of their large contribution to the weighted sum of squares of the linear**  
 300 **regression of the data. Top panel: Isotope correlation diagram combining stepped heating data from 6**  
 301 **individual crystal stepped heating experiments: 5 K-feldspar (ellipses) and 1 biotite (squares). The first**  
 302 **two biotite temperature steps were dominated by air and have been excluded from the diagrams for**  
 303 **clarity. Light grey symbols = low temperature steps ( $\sim 0.5\text{W}$ ), dark grey symbols = medium temperature**  
 304 **steps ( $\sim 1.5$  W) and black symbols = high temperature steps (4-10 W). Bottom panel: Isotope correlation**  
 305 **diagram of the single crystal fusion data. Ellipses = K-feldspar data, squares = biotite data. Filled symbols**  
 306 **show the data contributing to the grey isochron line ( $55.3 \pm 1.1$  ka) which is based on all of the single**  
 307 **crystal fusion data. Black symbols represent the data points thought to be least-contaminated by excess**  
 308  **$^{40}\text{Ar}$  (see main text on the unmixing model) and form an isochron with an age of  $50 \pm 3$  ka.**

309 Next we consider whether the single crystal total fusion data can improve our estimate of the eruption age.  
310 If we assume that each crystal contains a different amount of excess  $^{40}\text{Ar}$ , and that some crystals contain  
311 little or no excess  $^{40}\text{Ar}$  as shown by the step-heating experiments, we can treat the dataset as a mixture of  
312 populations with different apparent ages, and that the youngest coherent age population represents the  
313 crystals least contaminated with excess  $^{40}\text{Ar}$  and is a best-estimate of the eruption age.

314 To identify the youngest coherent age population, ages were initially analysed using the Isoplot unmixing  
315 tool (Ludwig, 2008), which is based on Sambridge and Compston's (1994) algorithms for deconvoluting  
316 mixtures of similar age zircon populations. These algorithms aim to determine the true number of age  
317 components, their age values, and their relative proportions using an iterative procedure; the exact values  
318 of the true age and relative proportions of the different populations are not directly recoverable and,  
319 instead, the model makes a best estimate of the ages and proportions, based on a maximised likelihood of  
320 the data representing multiple age components (Sambridge and Compston, 1994). The procedure begins  
321 with a guess of the number of age components (age populations) and returns an estimate of the ages (with  
322 error), relative proportions of those components and likelihood that the data are best described by those  
323 components (the likelihood is returned as the inverse log of the likelihood – the relative misfit parameter).  
324 The procedure is repeated using a different number of components until a minimum value for the relative  
325 misfit parameter is achieved. The model assumes that all populations have a Gaussian distribution. The  
326 relative proportions are calculated as the ratio of the areas beneath each population's distribution curve  
327 (Figure 6) (Sambridge and Compston, 1994).

328 Use of this model to fully assess our single crystal fusion data is a little problematic because of the  
329 requirement for a Gaussian age distribution; while we expect the analyses not contaminated with excess  
330  $^{40}\text{Ar}$  to approximate a Gaussian distribution, this is unlikely for the variable contaminated crystals and the  
331 actual spread of ages in this population is likely to include a substantial tail to older ages. To maximise the  
332 likelihood of the model giving meaningful results, we attempted to remove the non-Gaussian tail from the  
333 excess  $^{40}\text{Ar}$  contaminated population by excluding all ages greater than Wilson et al's (1992) initial age  
334 estimate of 64 ka. We also excluded the three youngest data (all of which gave geologically unreasonable

335 ages of <32 ka). For the remaining 22 data points, a minimum value for the relative misfit parameter  
336 (1.044) was achieved by invoking 2 populations with the youngest population estimated at  $47.9 \pm 2.1$  ka  
337 and formed by 55% of the data and the older population estimated at  $59.6 \pm 3.6$  ka and formed by 45% of  
338 the data (Figure 6).



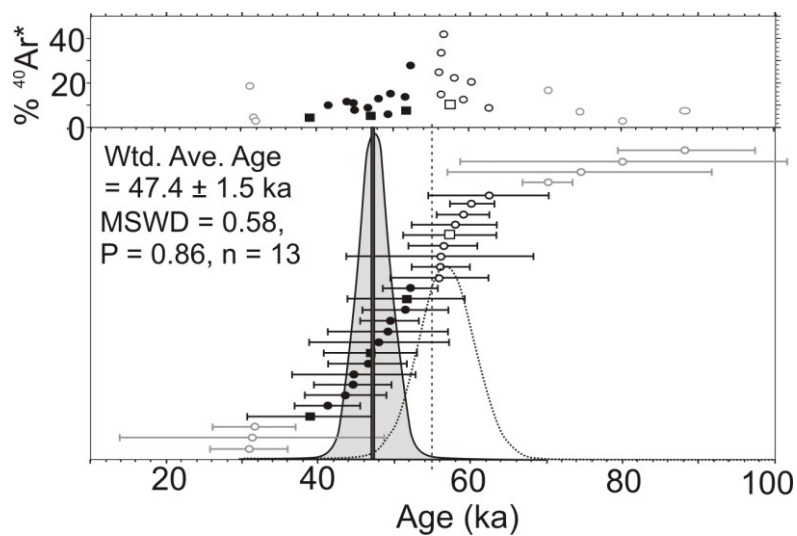
339

340 **Figure 6: Sambridge and Compston's (1994) unmixing model for the single crystal fusion  $^{40}\text{Ar}/^{39}\text{Ar}$  age**  
341 **data. Using Isoplot, the unmixing model suggests two populations are present: a younger population**  
342 **(estimated age  $47.9 \pm 2.1$  ka, 55%) and an older, excess  $^{40}\text{Ar}$  contaminated population (estimated age**  
343  **$59.6 \pm 3.6$  ka, 45%). The relative proportions of the populations are calculated by ratioing the area**  
344 **beneath the population curves. Where the curves overlap (grey shading), it is difficult to conclusively**  
345 **assign individual data points to each population. The diagram shows a hypothetical analysis with an age**  
346 **of 53 ka (dashed line) - the probability of this analysis belonging to the older population (f2) is greater**  
347 **than the probability of it belonging to the younger population (f1), but it could belong to either.**

348 This unmixing model was used to select analyses belonging to the youngest population from which to  
349 calculate a weighted average. Assigning each individual analysis to a population becomes difficult for ages  
350 that are described by both populations (shaded area on Figure 6). All ages > 52 ka (the point where the two  
351 population distribution curves cross) have a higher probability of belonging to the older population than  
352 the younger population (see case study of a hypothetical 53 ka data point in Figure 6). Simply assuming that  
353 the youngest 55% of the data (i.e. the youngest 12 analyses) represent the youngest population is likely to  
354 exclude data that do belong to the younger population, but have ages > 52 ka. Instead we consider the  
355 range of ages beneath the young population distribution curve as a guide to selecting data that are not

356 contaminated by excess  $^{40}\text{Ar}$  and use 55 ka as an upper limit for data belonging to the young population.  
 357 Using this criterion, 13 out of the 22 analyses were assigned to the young population ( $39 \pm 8$  to  $52 \pm 4$  ka). A  
 358 weighted average of these data gives an age of  $47.4 \pm 1.5$  ka with a statistically acceptable MSWD  
 359 (according to the criteria of Wendt and Carl, 1991) of 0.58 for  $n = 13$  and a probability of fit of 0.86. Figure 7  
 360 shows this weighted average in the context of the individual data, the distribution curves for the population  
 361 unmixing model, and our cut-off point for selecting data representative of the young population.

362



363

364 **Figure 7: Single crystal fusion ages (circles = K-feldspar, squares = biotite) shown with the age distribution**  
 365 **of the two populations identified by the unmixing model (curves) and the 55 ka cut-off for selecting**  
 366 **analyses belonging to the youngest population (dashed vertical line). Grey symbols are data excluded**  
 367 **from the unmixing analyses to allow an approximation of Gaussian distribution for the populations. Filled**  
 368 **symbols represent data assigned to the young population. Open symbols represent data contaminated**  
 369 **with excess  $^{40}\text{Ar}$  and thus yield ages older than the eruption. Circles = K-feldspar, squares = biotite. Black**  
 370 **vertical line is the weighted average  $\pm 1\sigma$  of the young population ( $n=13$ ). Error bars on individual**  
 371 **analyses are  $1\sigma$ .**

372 A further assessment of this age was carried out by plotting an isochron of the data assigned to the young  
 373 population, giving an age of  $50 \pm 3$  ka, a  $^{40}\text{Ar}/^{36}\text{Ar}$  intercept of  $297 \pm 2$ , and an MSWD of 0.5. Figure 5 (lower  
 374 panel) compares this isochron to the full single crystal fusion data set. This isochron age is indistinguishable  
 375 from both the weighted average age and the youngest population derived by the unmixing model. Visual  
 376 inspection of the single crystal fusion isochron plots in Figure 5 shows that the data thought to belong to

377 the young population form a trend that is qualitatively different from the other analyses, as would be  
378 expected when comparing an excess  $^{40}\text{Ar}$ -free population with data that are contaminated with excess  $^{40}\text{Ar}$ .

## 379 **5. Discussion and implications**

380 Our preferred estimate of the eruption age is the statistically robust weighted mean ( $47.4 \pm 1.5$  ka). It is  
381 consistent with a number of previously published ages for the Rotoiti eruption (Berryman, 1993, 1993;  
382 Buhay et al., 1992; Charlier et al., 2003; Danišík et al., 2012; Lian and Shane, 2000; Molloy et al., 2009;  
383 Nilsson et al., 2011; Santos et al., 2001; Shane et al., 2006; Shane and Sandiford, 2003), but is significantly  
384 younger than Wilson et al.'s (2007) age. The latter ( $61.0 \pm 1.4$  ka) is based on extrapolation between a K-Ar  
385 age for an underlying lava flow and a  $^{40}\text{Ar}/^{39}\text{Ar}$  age for an overlying obsidian lava flow ( $58.5 \pm 1.1$  ka) that  
386 bracket the Rotoehu ash on Mayor Island. Regardless of accuracy of Wilson et al.'s age extrapolation to the  
387 Rotoehu ash, the  $^{40}\text{Ar}/^{39}\text{Ar}$  age of the overlying lava flow should be younger than that of the Rotoiti  
388 eruption; this is not observed for our new eruption age and this discrepancy warrants discussion.

389 In addition to the overlying lava age, Wilson et al (2007) also report  $^{40}\text{Ar}/^{39}\text{Ar}$  ages from stepped heating  
390 experiments carried out on multi-grain aliquots of biotite and plagioclase separated from the Rotoiti  
391 Pumice, fused lithic clasts similar to the sample analysed in this study, and from the Earthquake Flat  
392 Pumice. While some of these ages clearly reflect contamination with excess or inherited  $^{40}\text{Ar}$ , others are  
393 comparable to Wilson et al.'s proposed eruption age. However, almost half of these ages overlap with our  
394 proposed eruption age at 2 standard deviations. Furthermore, as previously noted by Danišík et al. (2012),  
395 Wilson et al state that initial stepped heating experiments on biotites from fused lithics yielded younger  
396 isochron ages of 47 and 55 ka, but that these were discarded as they were at odds with the bracketing lava  
397 ages.

398 It seems the main discrepancy between our proposed age and that of Wilson et al (2007) concerns the ages  
399 of the overlying Mayor Island lava, which was determined on obsidian from the basal carapace. Either this  
400 obsidian age is too old or our K-feldspar and biotite ages are too young. To investigate if the discrepancy  
401 between our Rotoiti eruption age and Wilson et al's (2007) overlying lava flow age can be explained by

402 differences in assumed fluence monitor age, we recalculated both Mayor Island and Rotoiti eruption ages  
403 according to different monitor ages.

404 Wilson et al (2007) used Taylor Creek sanidine (TCs) as their neutron fluence, with an assumed age of 27.87  
405 Ma (Calvert and Lanphere, 2006), while we used ACs with an age of 1.1851 Ma (Rivera et al., 2013).

406 Published ages for TCs range from 27.87 – 28.62 ka (Duffield and Dalrymple, 1990; Karner and Renne, 1998;  
407 Kuiper et al., 2008; Renne et al., 2010; Sarna-Wojcicki et al., 2000), while recent published ACs ages range  
408 from  $1.180 \pm 0.0025$  Ma (Coble et al., 2011) to  $1.2056 \pm 0.0019$  Ma (Renne et al., 2011). Recalculating the  
409 Mayor Island obsidian flow using a TCs age of 28.62 Ma increases the obsidian age from 58.5 ka to 60.1 ka.  
410 Recalculating our 47.4 ka Rotoiti eruption age using ACs ages of 1.180 Ma and 1.2056 Ma gives ages of 47.2  
411 ka and 48.2 ka respectively. Our eruption age remains significantly younger than Wilson et al's age for the  
412 overlying lava and this discrepancy cannot be explained by differences in fluence monitor age.

413 Young apparent  $^{40}\text{Ar}/^{39}\text{Ar}$  ages may result from loss of  $^{40}\text{Ar}^*$  during reheating or alteration or by over-  
414 correction for atmospheric  $^{40}\text{Ar}$  by an apparent excess of  $^{36}\text{Ar}$ . Loss of radiogenic  $^{40}\text{Ar}^*$  during reheating is  
415 not thought to be an issue for our samples as these volcanic rocks have remained at the surface of the  
416 earth since they were erupted and so have not experienced subsequent heating events. While alteration  
417 may be an issue for a minority of analyses, our K-feldspar crystals were fresh with a glassy appearance and  
418 were often optically clear and euhedral while the biotite crystals appeared fresh and unaltered. Apparent  
419 excesses of  $^{36}\text{Ar}$  may occur due to isobaric interferences in the mass spectrometer from ( $^{12}\text{C}_3$ ) and ( $^1\text{H}^{35}\text{Cl}$ ).

420 We do not think this is likely as the Noblesse is able to partially resolve  $^{36}\text{Ar}$  from ( $^{12}\text{C}_3$ ) and mass 35 was  
421 measured for each analysis to monitor Cl contamination, but never yielded analyses greater than blank  
422 values. If a fractionated Ar-isotope component enriched in  $^{36}\text{Ar}$  were incorporated homogeneously into the  
423 crystals, this would result in younger individual apparent ages, but not affect the isochron ages and be  
424 detectable on isotope correlation diagrams. Inhomogeneous incorporation of excess  $^{36}\text{Ar}$  may not be  
425 detectable, but this fractionated component would also have to reside in the crystal lattice and be released  
426 at high-temperatures to reproduce the stepped heating data, which seems unlikely. Furthermore, excess  
427  $^{36}\text{Ar}$  has not been documented in crystalline materials before.

428 Whilst obsidian has been successfully used to produce geologically meaningful  $^{40}\text{Ar}/^{39}\text{Ar}$  ages (Flude et al.,  
429 2010; Morgan et al., 2009; Vogel et al., 2006), it is known to be problematic for reasons that are only just  
430 starting to become clear, and it is at least qualitatively possible that these poorly-understood processes can  
431 result in over-estimation of  $^{40}\text{Ar}/^{39}\text{Ar}$  age spectra and isochron ages. Brown et al. (2009) and Morgan et al.  
432 (2009) suggested that the Ar-isotope composition of obsidians in Ethiopia had been affected by kinetic  
433 isotope fractionation of atmospheric gas either prior to or during absorption, while Flude et al. (in prep)  
434 concluded that kinetic isotope fractionation during magmatic degassing produced heterogeneously  
435 distributed excess  $^{40}\text{Ar}$  due to preferential loss of  $^{36}\text{Ar}$  during degassing. As already discussed, when  
436 distributed heterogeneously, excess  $^{40}\text{Ar}$  may be difficult to detect via age spectra and isotope correlation  
437 diagrams (Kuiper, 2002; Sherlock and Arnaud, 1999), and this may be exacerbated when step-heating  
438 aliquots of crushed obsidian which may mix small-scale isotope reservoirs and destroy any naturally  
439 occurring isotope profiles that might be detected by stepped-heating of a single fragment (i.e. the  
440 laboratory diffusion dimension is less than the natural diffusion dimension). Furthermore, if kinetic isotopic  
441 fractionation were to take place during stepped heating of obsidian in the laboratory we would expect  $^{36}\text{Ar}$   
442 to be released faster than  $^{40}\text{Ar}$ , resulting in relative depression of  $^{40}\text{Ar}/^{36}\text{Ar}$  values in the earliest heating  
443 steps and elevation in the later heating steps. Isochrons from such data may give apparent ages that are  
444 too high with  $^{40}\text{Ar}/^{36}\text{Ar}$  intercepts that are too low, thus obscuring the presence of any excess  $^{40}\text{Ar}$  and  
445 yielding an incorrect but seemingly robust apparent  $^{40}\text{Ar}/^{39}\text{Ar}$  age.

446 We are unable to identify a mechanism that could result in our proposed eruption age being under-  
447 estimated by ~10-15 kyrs, but it is possible that Wilson et al's (2007) obsidian age is an over-estimate. We  
448 also note that our proposed eruption age is within error of many other age estimates for the Rotoiti  
449 eruption, is consistent with palaeoenvironmental interpretations (Shane and Sandiford, 2003), and that  
450 there are now three radio-isotope techniques ( $^{14}\text{C}$ , U-Th-He,  $^{40}\text{Ar}/^{39}\text{Ar}$ ) that have yielded consistent  
451 eruption ages ~ 45-47 ka. As previously discussed by Danišić et al. (2012), adopting a younger age for the  
452 Rotoiti eruption suggests that the TVZ has been much more active than previously realised. Revision

453 increases silicic magma production rates for the Okataina caldera complex from  $2.5 \text{ km}^3 \text{ ka}^{-1}$  (Wilson et al.,  
454 1995) to  $3.8 \text{ km}^3 \text{ ka}^{-1}$  and magma eruption rates of the TVZ are revised to  $\sim 17 \text{ km}^3 \text{ kyr}^{-1}$ .

## 455 **5. Conclusions**

456 Vapour phase crystallisation of K-feldspar and biotite in miarolytic cavities of glass-bearing granitoid clasts  
457 entrained in the eruption of the Rotoiti ignimbrite provide high-K phases suitable for  $^{40}\text{Ar}/^{39}\text{Ar}$  dating of this  
458 young, difficult to date eruption. Stepped-heating Ar-isotope analyses on single crystals indicate that excess  
459  $^{40}\text{Ar}$  is present in fluid and / or magmatic inclusions present in some of the crystals and is released at low  
460 temperatures. This excess  $^{40}\text{Ar}$  component is variable and not present in every crystal and so isotope  
461 correlation diagrams using single crystal fusion data represent mixing between three components of  $^{40}\text{Ar}$   
462 (radiogenic, atmospheric and excess) and do not provide accurate trapped Ar compositions or  $^{40}\text{Ar}/^{39}\text{Ar}$   
463 ages. An isochron of the stepped heating data is dominated by the moderate-high temperature heating  
464 steps and gives an upper limit of the eruption age of  $54 \pm 3 \text{ ka}$ .

465 The eruption age can be further refined by treating the single-crystal fusion data as a mixed population and  
466 assuming that the youngest cohesive age population represents the eruption age. A population unmixing  
467 model was used to identify a young population, free from excess  $^{40}\text{Ar}$  contamination. This population gave a  
468 statistically valid weighted mean eruption age of  $47.4 \pm 1.5 \text{ ka}$  which is indistinguishable from recent (U-  
469 Th)/He and  $^{14}\text{C}$  age determinations by Danišik et al. (2012) and from various other published age  
470 determinations based on marine and lake sedimentation rates. However, our new age is significantly  
471 younger than the  $^{40}\text{Ar}/^{39}\text{Ar}$  age for an obsidian lava flow overlying the Rotoehu ash on Mayor Island,  
472 presented by Wilson et al. (2007) and this discrepancy may be explained by kinetic fractionation of Ar-  
473 isotopes in obsidian both in nature and the laboratory.

## 474 **Acknowledgements**

475 Fieldwork in New Zealand was carried out by MS during tenure of a 1-year fellowship at the University of  
476 Waikato. The Quaternary Dating Laboratory at Roskilde University is funded by the Villum Foundation. This



477 manuscript benefitted from comments and discussion by reviewers Andy Calvert and an anonymous  
478 reviewer, and Editor Paul Renne.

## 479 References

- 480 Allan, A.S.R., Baker, J.A., Carter, L., Wysoczanski, R.J., 2008. Reconstructing the Quaternary evolution of the  
481 world's most active silicic volcanic system: insights from an ~1.65 Ma deep ocean tephra record  
482 sourced from Taupo Volcanic Zone, New Zealand. *Quaternary Science Reviews* 27, 2341–2360.  
483 doi:10.1016/j.quascirev.2008.09.003
- 484 Berryman, K., 1992. A stratigraphic age of Rotoehu Ash and late Pleistocene climate interpretation based  
485 on marine terrace chronology, Mahia Peninsula, North Island, New Zealand. *New Zealand Journal*  
486 *of Geology and Geophysics* 35, 1–7. doi:10.1080/00288306.1992.9514494
- 487 Berryman, K.R., 1993. Distribution, age, and deformation of Late Pleistocene marine terraces at Mahia  
488 Peninsula, Hikurangi Subduction Margin, New Zealand. *Tectonics* 12, 1365–1379.  
489 doi:10.1029/93TC01543
- 490 Brown, F.H., Reid, C., Negash, A., 2009. Possible isotopic fractionation of argon in source obsidians and  
491 archeological artifacts from Kulkuletti, Ethiopia. *Journal of Archaeological Science* 36, 2119–2124.  
492 doi:10.1016/j.jas.2009.05.008
- 493 Brown, S.J., Burt, R., Cole, J., Krippner, S.J., Price, R., Cartwright, I., 1998. Plutonic lithics in ignimbrites of  
494 Taupo Volcanic Zone, New Zealand; sources and conditions of crystallisation. *Chemical Geology*  
495 148, 21–41. doi:10.1016/S0009-2541(98)00026-6
- 496 Brumm, A., Jensen, G.M., van den Bergh, G.D., Morwood, M.J., Kurniawan, I., Aziz, F., Storey, M., 2010.  
497 Hominins on Flores, Indonesia, by one million years ago. *Nature* 464, 748–752.  
498 doi:10.1038/nature08844
- 499 Buhay, W.M., Clifford, P.M., Schwarcz, H.P., 1992. ESR dating of the Rotoiti Breccia in the Taupo volcanic  
500 zone, New Zealand. *Quaternary Science Reviews* 11, 267–271. doi:10.1016/0277-3791(92)90072-G
- 501 Burt, R.M., Brown, S.J.A., Cole, J.W., Shelley, D., Waight, T.E., 1998. Glass-bearing plutonic fragments from  
502 ignimbrites of the Okataina caldera complex, Taupo Volcanic Zone, New Zealand: remnants of a  
503 partially molten intrusion associated with preceding eruptions. *Journal of Volcanology and*  
504 *Geothermal Research* 84, 209–237. doi:10.1016/S0377-0273(98)00039-0
- 505 Calvert, A.T., Lanphere, M.A., 2006. Argon geochronology of Kilauea's early submarine history. *Journal of*  
506 *Volcanology and Geothermal Research* 151, 1–18. doi:10.1016/j.jvolgeores.2005.07.023
- 507 Chappell, J., 2002. Sea level changes forced ice breakouts in the Last Glacial cycle: new results from coral  
508 terraces. *Quaternary Science Reviews* 21, 1229–1240. doi:10.1016/S0277-3791(01)00141-X
- 509 Chappell, J., Shackleton, N.J., 1986. Oxygen isotopes and sea level. *Nature* 324, 137–140.  
510 doi:10.1038/324137a0
- 511 Charlier, B.L.A., Wilson, C.J.N., 2010. Chronology and Evolution of Caldera-forming and Post-caldera Magma  
512 Systems at Okataina Volcano, New Zealand from Zircon U-Th Model-age Spectra. *Journal of*  
513 *Petrology* 51, 1121–1141. doi:10.1093/petrology/egq015
- 514 Charlier, B.L., Peate, D.W., Wilson, C.J., Lowenstern, J.B., Storey, M., Brown, S.J., 2003. Crystallisation ages  
515 in coeval silicic magma bodies: 238U–230Th disequilibrium evidence from the Rotoiti and  
516 Earthquake Flat eruption deposits, Taupo Volcanic Zone, New Zealand. *Earth and Planetary Science*  
517 *Letters* 206, 441–457. doi:10.1016/S0012-821X(02)01109-3
- 518 Coble, M.A., Grove, M., Calvert, A.T., 2011. Calibration of Nu-Instruments Noblesse multicollector mass  
519 spectrometers for argon isotopic measurements using a newly developed reference gas. *Chemical*  
520 *Geology* 290, 75–87. doi:10.1016/j.chemgeo.2011.09.003
- 521 Danišik, M., Shane, P., Schmitt, A.K., Hogg, A., Santos, G.M., Storm, S., Evans, N.J., Keith Fifield, L., Lindsay,  
522 J.M., 2012. Re-anchoring the late Pleistocene tephrochronology of New Zealand based on  
523 concordant radiocarbon ages and combined 238U/230Th disequilibrium and (U–Th)/He zircon ages.  
524 *Earth and Planetary Science Letters* 349–350, 240–250. doi:10.1016/j.epsl.2012.06.041
- 525 Duffield, W., Dalrymple, G., 1990. The Taylor Creek Rhyolite of New Mexico: a rapidly emplaced field of  
526 lava domes and flows. *Bull Volcanol* 52, 475–487. doi:10.1007/BF00268927

527 Ewart, A., Cole, J.W., 1967. Textural and mineralogical significance of the Granitic Xenoliths from the  
528 Central Volcanic Region, North Island, New Zealand. *New Zealand Journal of Geology and*  
529 *Geophysics* 10, 31–54. doi:10.1080/00288306.1967.10428183

530 Flude, S., McGarvie, D.W., Burgess, R., Tindle, A.G., 2010. Rhyolites at Kerlingarfjöll, Iceland: the evolution  
531 and lifespan of silicic central volcanoes. *Bulletin of Volcanology* 72, 523–538. doi:10.1007/s00445-  
532 010-0344-0

533 Flude, S., Tuffen, H., Sherlock, S.C., Kelley, S.P., in prep. Excess  $^{40}\text{Ar}$  in obsidian from Ar-isotope  
534 fractionation during magmatic degassing.

535 Foland, K.A., 1994. Argon diffusion in feldspars, in: Parsons, I. (Ed.), *Feldspars and Their Reactions*. Kluwer  
536 Academic Publishers.

537 Froggatt, P.C., Lowe, D.J., 1990. A review of late Quaternary silicic and some other tephra formations from  
538 New Zealand: Their stratigraphy, nomenclature, distribution, volume, and age. *New Zealand*  
539 *Journal of Geology and Geophysics* 33, 89–109. doi:10.1080/00288306.1990.10427576

540 Grant-Taylor, T.L., Rafter, T.A., 1971. New Zealand radiocarbon age measurements — 6. *New Zealand*  
541 *Journal of Geology and Geophysics* 14, 364–402. doi:10.1080/00288306.1971.10421932

542 Jourdan, F., Matzel, J.P., Renne, P.R., 2007.  $^{39}\text{Ar}$  and  $^{37}\text{Ar}$  recoil loss during neutron irradiation of sanidine  
543 and plagioclase. *Geochimica et Cosmochimica Acta* 71, 2791–2808. doi:10.1016/j.gca.2007.03.017

544 Karner, D.B., Renne, P.R., 1998.  $^{40}\text{Ar}/^{39}\text{Ar}$  geochronology of Roman volcanic province tephra in the Tiber  
545 River valley: Age calibration of middle Pleistocene sea-level changes. *Geological Society of America*  
546 *Bulletin* 110, 740–747. doi:10.1130/0016-7606(1998)110<0740:AAGORV>2.3.CO;2

547 Kimber, R.W.L., Kennedy, N.M., Milnes, A.R., 1994. Amino acid racemization dating of a 140 000 year old  
548 tephra-loess-palaeosol sequence on the Mamaku Plateau near Rotorua, New Zealand. *Australian*  
549 *Journal of Earth Sciences* 41, 19–26. doi:10.1080/08120099408728109

550 Kuiper, K.F., Deino, A., Hilgen, F.J., Krijgsman, W., Renne, P.R., Wijbrans, J.R., 2008. Synchronizing Rock  
551 Clocks of Earth History. *Science* 320, 500–504. doi:10.1126/science.1154339

552 Kuiper, Y.D., 2002. The interpretation of inverse isochron diagrams in  $^{40}\text{Ar}/^{39}\text{Ar}$  geochronology. *Earth and*  
553 *Planetary Science Letters* 203, 499–506. doi:10.1016/S0012-821X(02)00833-6

554 Lian, O.B., Shane, P.A., 2000. Optical dating of paleosols bracketing the widespread Rotoehu tephra, North  
555 Island, New Zealand. *Quaternary Science Reviews* 19, 1649–1662. doi:10.1016/S0277-  
556 3791(00)00003-2

557 Lofgren, G.E., Gooley, R., 1977. Simultaneous crystallization of feldspar intergrowths from the melt.  
558 *American Mineralogist* 62, 217–228.

559 Lowe, D.J., Hogg, A.G., 1995. Letter to the Editor: Age of the Rotoehu Ash Comment. *New Zealand Journal*  
560 *of Geology and Geophysics* 38, 399–402. doi:10.1080/00288306.1995.9514666

561 Ludwig, K.R., 2008. User's manual for Isoplot 3.7: A geochronological Toolkit for Microsoft Excel.

562 McDougall, I., Harrison, T.M., 1999. *Geochronology and Thermochronology by the  $^{40}\text{Ar}/^{39}\text{Ar}$  method*, 2nd  
563 Edition. ed. Oxford University Press.

564 Mcglone, M.S., Howorth, R., Pullar, W.A., 1984. Late Pleistocene stratigraphy, vegetation and climate of the  
565 Bay of Plenty and Gisborne regions, New Zealand. *New Zealand Journal of Geology and Geophysics*  
566 27, 327–350.

567 Molloy, C., Shane, P., Augustinus, P., 2009. Eruption recurrence rates in a basaltic volcanic field based on  
568 tephra layers in maar sediments: Implications for hazards in the Auckland volcanic field. *Geological*  
569 *Society of America Bulletin* 121, 1666–1677. doi:10.1130/B26447.1

570 Molloy, C., Shane, P., Nairn, I., 2008. Pre-eruption thermal rejuvenation and stirring of a partly crystalline  
571 rhyolite pluton revealed by the Earthquake Flat Pyroclastics deposits, New Zealand. *Journal of the*  
572 *Geological Society* 165, 435–447. doi:10.1144/0016-76492007-071

573 Morgan, L.E., Renne, P.R., Taylor, R.E., WoldeGabriel, G., 2009. Archaeological age constraints from  
574 extrusion ages of obsidian: Examples from the Middle Awash, Ethiopia. *Quaternary Geochronology*  
575 4, 193–203. doi:10.1016/j.quageo.2009.01.001

576 Nairn, I.A., Kohn, B.P., 1973. Relation of the Earthquake Flat Breccia to the Rotoiti Breccia, Central North  
577 Island, New Zealand. *New Zealand Journal of Geology and Geophysics* 16, 269–279.  
578 doi:10.1080/00288306.1973.10431457

579 Nathan, S., 1976. Age of the Rotoiti Breccia formation. Geological Society of New Zealand newsletter 41,  
580 21–24.

581 Nilsson, A., Muscheler, R., Snowball, I., Aldahan, A., Possnert, G., Augustinus, P., Atkin, D., Stephens, T.,  
582 2011. Multi-proxy identification of the Laschamp geomagnetic field excursion in Lake Pupuke, New  
583 Zealand. Earth and Planetary Science Letters 311, 155–164. doi:10.1016/j.epsl.2011.08.050

584 Ota, Y., Omura, A., Iwata, H., 1989. <sup>230</sup>Th-<sup>238</sup>U age of Rotoehu Ash and its implications for marine terrace  
585 chronology of eastern Bay of Plenty, New Zealand. New Zealand Journal of Geology and Geophysics  
586 32, 327–331. doi:10.1080/00288306.1989.10425712

587 Pillans, B., Wright, I., 1992. Late Quaternary tephrostratigraphy from the southern Havre Trough - Bay of  
588 Plenty, northeast New Zealand. New Zealand Journal of Geology and Geophysics 35, 129–143.  
589 doi:10.1080/00288306.1992.9514507

590 Pullar, W.A., 1976. Age of Rotoiti Breccia Formation. Geological Society of New Zealand newsletter 41, 22–  
591 23.

592 Pullar, W.A., Heine, J.C., 1971. Ages, inferred from <sup>14</sup>C dates, of some tephra and other deposits from  
593 Rotorua, Taupo, Bay of Plenty and Hawke’s Bay districts. Proceedings of Radiocarbon User’s  
594 Conference, Lower Hitt 118–138.

595 Pullar, W.A., Nairn, I.A., 1972. Matahi Basaltic Tephra member, Rotoiti Breccia Formation. New Zealand  
596 Journal of Geology and Geophysics 15, 446–450. doi:10.1080/00288306.1972.10422342

597 Renne, P.R., Balco, G., Ludwig, K.R., Mundil, R., Min, K., 2011. Response to the comment by W.H. Schwarz et  
598 al. on “Joint determination of 40K decay constants and 40Ar\*/40K for the Fish Canyon sanidine  
599 standard, and improved accuracy for 40Ar/39Ar geochronology” by P.R. Renne et al. (2010).  
600 Geochimica et Cosmochimica Acta 75, 5097–5100. doi:10.1016/j.gca.2011.06.021

601 Renne, P.R., Mundil, R., Balco, G., Min, K., Ludwig, K.R., 2010. Joint determination of 40K decay constants  
602 and 40Ar\*/40K for the Fish Canyon sanidine standard, and improved accuracy for 40Ar/39Ar  
603 geochronology. Geochimica et Cosmochimica Acta 74, 5349–5367. doi:10.1016/j.gca.2010.06.017

604 Rivera, T.A., Storey, M., Schmitz, M.D., Crowley, J.L., 2013. Age intercalibration of 40Ar/39Ar sanidine and  
605 chemically distinct U/Pb zircon populations from the Alder Creek Rhyolite Quaternary  
606 geochronology standard. Chemical Geology 345, 87–98. doi:10.1016/j.chemgeo.2013.02.021

607 Sambridge, M.S., Compston, W., 1994. Mixture modeling of multi-component data sets with application to  
608 ion-probe zircon ages. Earth and Planetary Science Letters 128, 373–390. doi:10.1016/0012-  
609 821X(94)90157-0

610 Santos, G.M., Bird, M.I., Fifield, L.K., Alloway, B.V., Chappell, J., Hausladen, P.A., Arneith, A., 2001.  
611 Radiocarbon dating of wood using different pretreatment procedures; application to the  
612 chronology of Rotoehu Ash, New Zealand. Radiocarbon 43, 239–248.

613 Sarna-Wojcicki, A.M., Pringle, M.S., Wijbrans, J., 2000. New <sup>40</sup>Ar/<sup>39</sup>Ar age of the Bishop Tuff from multiple  
614 sites and sediment rate calibration for the Matuyama-Brunhes boundary. Journal of Geophysical  
615 Research 105, 21431. doi:10.1029/2000JB900901

616 Shane, P., 2000. Tephrochronology: a New Zealand case study. Earth-Science Reviews 49, 223–259.  
617 doi:10.1016/S0012-8252(99)00058-6

618 Shane, P., Nairn, I.A., Smith, V.C., 2005. Magma mingling in the ~50 ka Rotoiti eruption from Okataina  
619 Volcanic Centre: implications for geochemical diversity and chronology of large volume rhyolites.  
620 Journal of Volcanology and Geothermal Research 139, 295–313.  
621 doi:10.1016/j.jvolgeores.2004.08.012

622 Shane, P., Sandiford, A., 2003. Paleovegetation of marine isotope stages 4 and 3 in northern new zealand  
623 and the age of the widespread rotoehu tephra. Quaternary Research 59, 420–429.  
624 doi:10.1016/S0033-5894(03)00044-9

625 Shane, P., Sikes, E.L., Guilderson, T.P., 2006. Tephra beds in deep-sea cores off northern New Zealand:  
626 implications for the history of Taupo Volcanic Zone, Mayor Island and White Island volcanoes.  
627 Journal of Volcanology and Geothermal Research 154, 276–290.  
628 doi:10.1016/j.jvolgeores.2006.03.021

629 Shane, P., Storm, S., Schmitt, A.K., Lindsay, J.M., 2012. Timing and conditions of formation of granitoid  
630 clasts erupted in recent pyroclastic deposits from Tarawera Volcano (New Zealand). Lithos 140–  
631 141, 1–10. doi:10.1016/j.lithos.2012.01.012

- 632 Sherlock, S.C., Arnaud, N.O., 1999. Flat plateau and impossible isochrons: apparent  $^{40}\text{Ar}$ - $^{39}\text{Ar}$   
633 geochronology in a high-pressure terrain. *Geochimica et Cosmochimica Acta* 63, 2835–2838.  
634 doi:10.1016/S0016-7037(99)00116-7
- 635 Smith, V., Shane, P., Nairn, I., 2010. Insights into silicic melt generation using plagioclase, quartz and melt  
636 inclusions from the caldera-forming Rotoiti eruption, Taupo volcanic zone, New Zealand. *Contrib*  
637 *Mineral Petrol* 160, 951–971. doi:10.1007/s00410-010-0516-0
- 638 Thompson, B.N., 1968a. Notes from the New Zealand Geological Survey—5: Age of Rotoiti Breccia. *New*  
639 *Zealand Journal of Geology and Geophysics* 11, 1189–1191. doi:10.1080/00288306.1968.10420248
- 640 Thompson, B.N., 1968b. Notes from the New Zealand Geological Survey—5: Age of Rotoiti Breccia. *New*  
641 *Zealand Journal of Geology and Geophysics* 11, 1189–1191. doi:10.1080/00288306.1968.10420248
- 642 Vogel, N., Nomade, S., Negash, A., Renne, P.R., 2006. Forensic  $^{40}\text{Ar}/^{39}\text{Ar}$  dating: a provenance study of  
643 Middle Stone Age obsidian artifacts from Ethiopia. *Journal of Archaeological Science* 33, 1749–  
644 1765. doi:10.1016/j.jas.2006.03.008
- 645 Vucetich, C.G., Pullar, W.A., 1969. Stratigraphy and chronology of late pleistocene volcanic ash beds in  
646 Central North Island, New Zealand. *New Zealand Journal of Geology and Geophysics* 12, 784–837.  
647 doi:10.1080/00288306.1969.10431112
- 648 Wendt, I., Carl, C., 1991. The statistical distribution of the mean squared weighted deviation. *Chemical*  
649 *Geology: Isotope Geoscience section* 86, 275–285. doi:10.1016/0168-9622(91)90010-T
- 650 Whitehead, N., Ditchburn, R., 1994. Revision of some ages for the Rotoehu Ash. *New Zealand Journal of*  
651 *Geology and Geophysics* 37, 381–383. doi:10.1080/00288306.1994.9514627
- 652 Wilson, C.J.N., Houghton, B.F., Lanphere, M.A., Weaver, S.D., 1992. A new radiometric age estimate for the  
653 Rotoehu Ash from Mayor Island volcano, New Zealand. *New Zealand Journal of Geology and*  
654 *Geophysics* 35, 371–374. doi:10.1080/00288306.1992.9514530
- 655 Wilson, C.J.N., Houghton, B.F., McWilliams, M.O., Lanphere, M.A., Weaver, S.D., Briggs, R.M., 1995.  
656 Volcanic and structural evolution of Taupo Volcanic Zone, New Zealand: a review. *Journal of*  
657 *Volcanology and Geothermal Research* 68, 1–28. doi:10.1016/0377-0273(95)00006-G
- 658 Wilson, C.J.N., Rhoades, D.A., Lanphere, M.A., Calvert, A.T., Houghton, B.F., Weaver, S.D., Cole, J.W., 2007.  
659 A multiple-approach radiometric age estimate for the Rotoiti and Earthquake Flat eruptions, New  
660 Zealand, with implications for the MIS 4/3 boundary. *Quaternary Science Reviews* 26, 1861–1870.  
661 doi:10.1016/j.quascirev.2007.04.017  
662